TECHNICAL SCIENCES

FEATURES OF PHYSICAL AND METALLURGICAL PROCESSES DURING WELDING OF THIN-WALLED ALUMINUM ALLOY STRUCTURES USING LASER RADIATION

https://doi.org/10.5281/zenodo.7271299

Peleshenko S.,
NTUU "Igor Sikorsky Kyiv Polytechnic Institute", Kyiv, Ukraine
Kvasnytskyi V.,
NTUU "Igor Sikorsky Kyiv Polytechnic Institute", Kyiv, Ukraine
Khaskin V.,
The Paton Electric Welding Institute of the NASU, Kyiv, Ukraine
Korzhyk V.,
The Paton Electric Welding Institute of the NASU, Kyiv, Ukraine
Illyashenko Ye.,
The Paton Electric Welding Institute of the NASU, Kyiv, Ukraine
Lepilina K.,
The Paton Electric Welding Institute of the NASU, Kyiv, Ukraine
Aloshyn A.
The Paton Electric Welding Institute of the NASU, Kyiv, Ukraine

Abstract

This paper aims to study features of physical and metallurgical processes during welding of thin-walled structures made of aluminum alloys using laser radiation, including the effect of concomitant heating provided by a compressed electric arc of direct action, as well as the influence of distance between a center of anode region of compressed arc of a non-consumable electrode and an axis of laser radiation, on reduction of laser energy losses. To perform the study, modes of laser and laser-plasma welding are selected and correspondent experiments are carried out to determine the effect of specified distance, as well as metallographic analysis of experimental results is made. It is determined that applying the concomitant plasma heating in laser welding makes it possible to increase the penetration depth by 15–65% compared to conventional laser welding, including by improving radiation absorption. To improve absorption of radiation during laser-plasma welding, it is recommended that distance between a center of anode region of compressed arc of a non-consumable electrode and an axis of laser radiation should not exceed 1.0 mm, and in hybrid welding it should not exceed 0.5 mm. During laser welding of 7075 alloy, it is possible to obtain joints with sufficiently narrow seams with minimal energy input and lifetime of a melt pool. However, typical defects such as microcracks 10 –20 μm long in HAZ and oxide film inclusions in the root part of the remelted metal may occur. The use of concomitant local plasma heating during laser welding of 7075 alloy may provide reduction in graininess and increase in uniformity of hardness of joints in combination with elimination of formation of microcracks and oxide inclusions, which makes laser-plasma welding method more preferred.

Keywords: laser radiation, absorption, welding, hybrid, laser-plasma, aluminum alloys, structures.

1. Introduction.

One of the urgent tasks of modern science and technology is the creation of intelligent technologies and manufacturing processes. In particular, one of the most urgent tasks is the development of intelligent welding technologies based on the use of neural networks to control the concentration of thermal energy that is transferred into metal [1, 2]. To implement such technologies, it is recommended to use an intelligent automated system for monitoring and processing information (Fig. 1). This approach makes it possible to ensure the required welding productivity, the quality of the obtained welded joint, as well as process stability and reproducibility of its results.

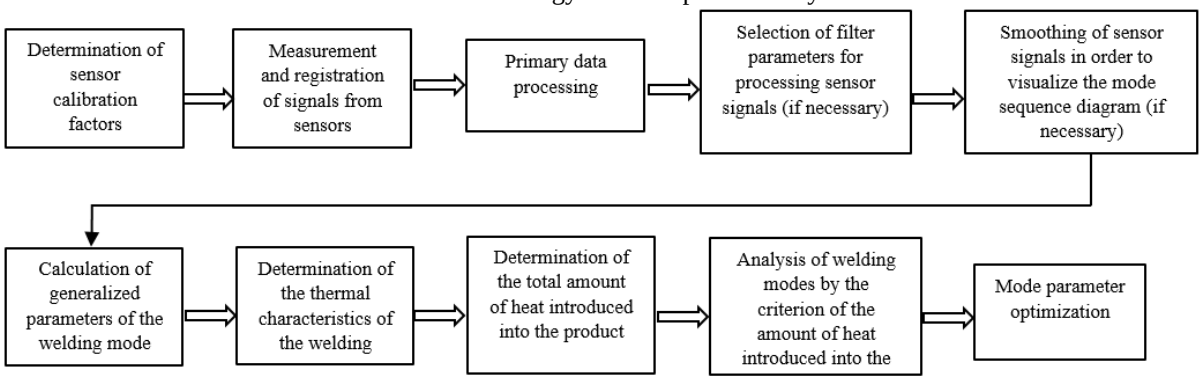

Fig.1. – Algorithm of digital signal processing during analysis and optimization of welding technology modes.

In recent years, laser and hybrid laser-plasma sources have been increasingly used as a controlled heat source for welding metal materials. In laser-plasma welding, a focused laser beam and a compressed electric arc have a joint thermal effect on the metal being welded within the common heating zone [3]. At the same time, the regularities of the mutual influence of the components of a laser-plasma heat source and their joint effect on various metallic materials have not yet been studied enough [4]. The study of the physics of the processes of interaction of the components of a laser-arc source with each other and their combined effect on the welded metal, the development of appropriate mathematical models and computer simulation of these processes have become important scientific-technical tasks.

When solving the problems of welding of thin-walled structures made of aluminum alloys using laser radiation, it is necessary to take into account the features of physical and metallurgical processes in the weld pool [5]. For example, during laser welding, a significant reflection of laser radiation is observed. This is due to the impact of a moving laser beam on unmolten metal during the welding process. Such metal has a low absorption coefficient of laser radiation *A*. This coefficient increases abruptly when the melting temperature *T* of the welded metal is reached (Fig. 2). Therefore, laser radiation losses can be reduced by using concomitant heating, for example, by arc plasma in hybrid laser-plasma processes [6].

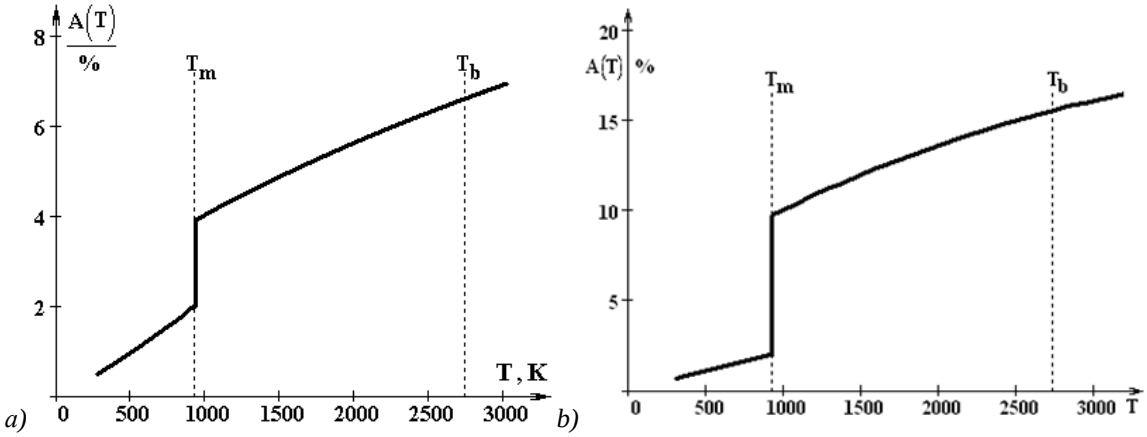

Fig. 2. – Dependences of aluminum absorption capacity A [%] on temperature T [K] [6]: a) – for laser radiation wavelength λ=10.6 μm; b) for laser radiation wavelength λ=1.06 μm.

This approach may increase the productivity of welding by increasing the effective efficiency, i.e., increasing the ratio of power of a heat source, which is acting in the metal during welding, to a total power of the compressed electric arc and laser radiation. Thus, one of the most promising ways to increase the efficiency of welding is to reduce laser energy losses associated with the reflection of radiation from the surface being welded [7].

2. Purpose and tasks.

The purpose of this study is to determine the features of physical and metallurgical processes during welding of thin-walled structures made of aluminum alloys using laser radiation, including the effect of concomitant heating provided by a compressed electric arc of direct action, as well as the effect of the distance between the center of the anode region of the compressed arc of a non-consumable electrode and the axis of laser radiation to reduce the loss of laser energy.

To achieve the aim, the following tasks are solved:

- determination of influence of the distance between the anode region of the compressed arc of the non-consumable electrode and the axis of laser radiation on the efficiency of absorption of laser radiation by metal being welded;

- determination of metallurgical features of formation of high-strength aluminum alloy joints by laser welding method;

- determination of metallurgical features of formation of high-strength aluminum alloy joints by laser-plasma welding method.

3. Materials and methods.

Experiments on laser and laser-plasma welding were carried out according to the schemes shown in Fig.3. To implement the experiments, a laser-plasma welding head was developed, which is shown in Fig. 4. Plates of 7075 alloy with sizes of 100×50×1.5 mm and higher were used as welded samples. Welding was performed with incomplete penetration to a depth of 0.5-0.7 mm. A fiber laser (λ≈1.06 μm) with a power of up to 2.0 kW was used as a radiation source. To generate direct arc plasma, a power source of unique design with current regulation of up to 80 A was used.

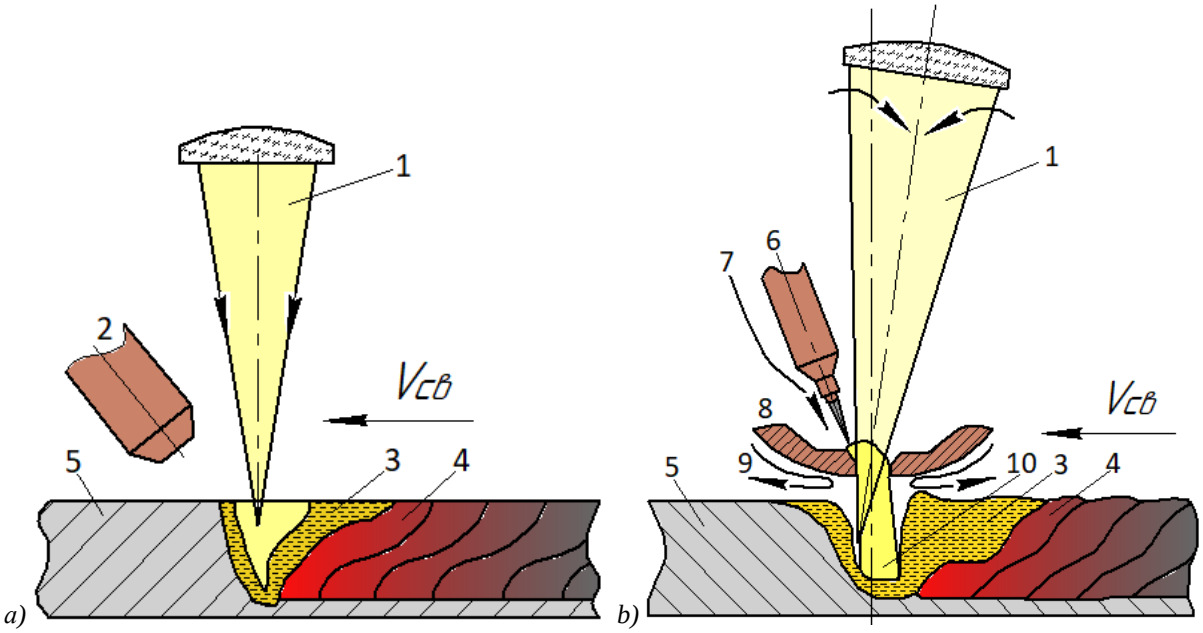

Fig. 3. – Scheme of laser (a) and hybrid laser-plasma (b) welding: 1 – focused laser radiation; 2 – protective nozzle; 3 – welding pool; 4 – weld metal; 5 – base metal; 6 – non-consumable electrode; 7 – plasma gas; 8 – plasma nozzle; 9 – shielding gas; 10 – plasma of direct action.

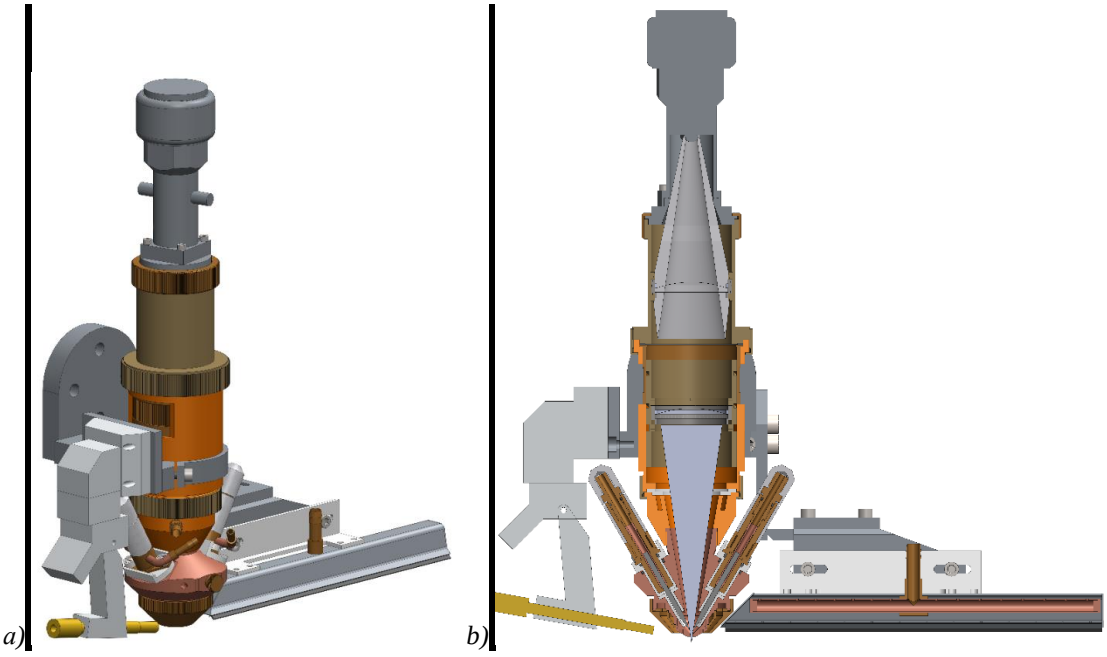

c)

Fig.4.
3D-model (a, b) and appearance (c) of the head for laser and laser-plasma welding of aluminum alloy samples.

In the case of laser-plasma welding, it was possible to change the distance *L* between the focusing point (axis) of laser radiation and the conditional point of the center of the anode spot. The value of *L* was changed within 0-2 mm due to the deflection of the plasma arc by the flow of the plasma-forming gas. In this case, the compressed electric arc was located on the side and somewhat ahead in the course of welding relative to the focused laser radiation. A plate made of 5083 alloy with a thickness of δ=2 mm was used as a sample for making penetrations. In the course of the experiments, the laser radiation power P_L was changed and, in each case, the penetration depth h was determined. At the same time, the effectiveness of the influence of concomitant plasma heating on the penetration depth and welding speed was studied.

The following technique was adopted in the work for obtaining and studying welded joints from high-strength aluminum alloy 7075:

- selection of mode parameters according to the criterion of forming a joint of the best quality and performing welding by selected methods;
- production of templates for metallographic studies by optical and analytical scanning electron microscopy;
- determination of the dimensions of the remelted part of the metal, the heat-affected zone (HAZ) and the size of the metal grains in these zones;
- measurement of microhardness (at 1/3 of the penetration depth) at a load of 100 g, determination of the structure, structural features and defects of the metal in the remelted part and HAZ;
- determination of the presence of oxide inclusions and changes in the content of Mg, Mn, Zn in the metal of the remelted part and the HAZ in comparison with the base metal;
- determination of the presence and size of internal pores and cracks, as well as the causes of their occurrence.

To carry out experiments on selecting the modes of laser, plasma, and hybrid laser-plasma welding, samples of high-strength 7075 alloy were made. Analytical scanning microscopy was used to measure individual elements of the alloy to determine the change in their content under the action of focused laser radiation.

The choice of welding mode parameters was carried out according to the criteria of the qualitative formation of the upper weld bead, obtaining the required depth of penetration and the absence of visible cracks. Main parameters of the modes are given in Table 1.

Table 1.

Main parameters of welding modes for samples from 7075 alloy.

Welding method	Linear energy E, J/mm	Welding speed V, mm/s	Gas consumption (Ar), l/min	
			Plasma-forming	Shielding
Laser	5	50,0	–	8
Laser-plasma	15	66,7	10	30

The grain size Dg was determined using optical microscopy as the ratio of its height h to length l. In the base metal, the grain size is Dg = (10…20)×(25…70) μm, shape factor $\varnothing$ = l/h = 2.5…3.5. Microhardness HV at a load of 100 g is within 1100…1240 MPa. Segregations of the line type l_B=15…35 μm were revealed in the form of chains 35…75 μm in size (Fig. 5).

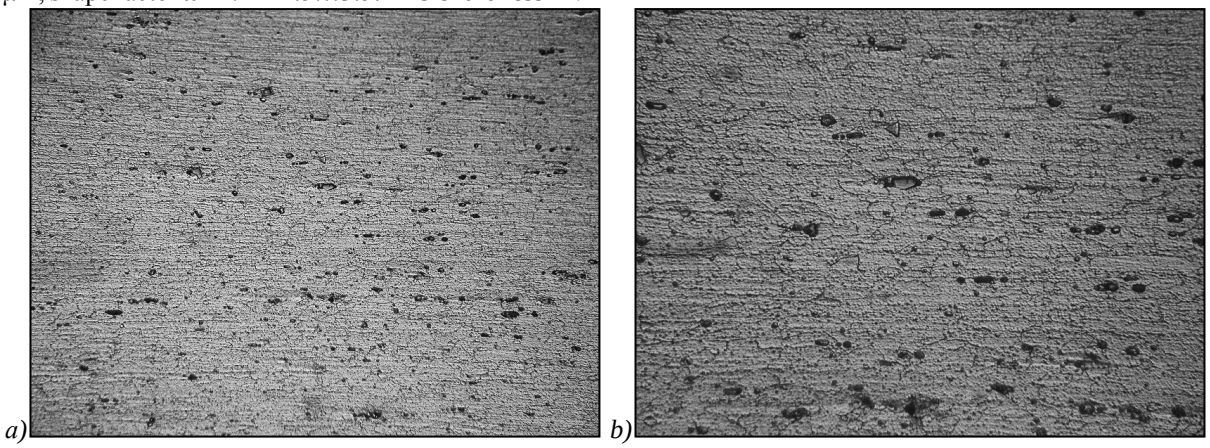

a) *b)*

Fig.5. – Structure of the base metal (alloy 7075) at ×250 (a) and ×500 (b) magnifications.

For metallographic analysis, the transverse templates were cut from the obtained joints and microsections were made. The ion-vacuum etching was applied during the analysis. The results of the connections made were studied by optical (Versamet-2 (UNITRON, USA) and Neophot-31 (Germany) microscopes) and analytical scanning electron microscopy (SEM-515 microscope, PHILIPS, Holland). The studies were carried out on the following sections of the samples: remelted weld metal → fusion line → HAZ → base metal. Structural changes were studied using optical microscopy. Microhardness was measured using an LM-400 microhardness tester (Leco Corporation, USA). Using analytical scanning electron microscopy, the chemical composition was determined (general and local spot analysis).

4. Results of experimental studies.

4.1. Determination of the influence of the parameter L on the efficiency of radiation absorption by the metal being welded.

To determine the influence of the distance between the focusing point of laser radiation and the conditional exact center of the anode region of the compressed arc on the process of laser-plasma welding, correspondent studies were carried out, in which the compressed plasma arc was deflected away from the laser beam using a plasma-forming gas (Table 2). Analysis of the obtained results showed the following. At values $L > 0.9…1.0$ mm, separate action of laser radiation and plasma was observed. Joint action was observed at $L < 0.9$ mm. A full-fledged hybrid laser-plasma process took place at $L < 0.5$ mm. Further analysis made it possible to build the dependencies shown in Fig.6. These dependences show that the use of concomitant plasma heating makes it possible to increase the welding speed by 25% compared to conventional laser method. In this case, the penetration depth of laser-plasma welding increases by 10-50%. Such results indirectly indicate an increase in the absorption of laser radiation by aluminum alloys during their local concomitant heating, for example, by compressed arc plasma.

Table 2.

The results of welding of 5083 plates (δ=2 mm) using hybrid method (1 – laser penetration P_L = 400 W, 2 – plasma penetration I = 50 A, U = 26 V) with different values of parameter L.

№	L, mm	Appearance of welds
1.	> 1,5	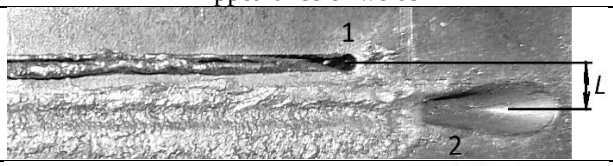
2.	1,5	
3.	1,0	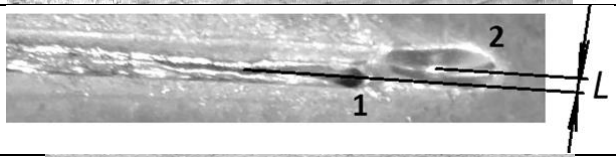
4.	< 0,5 мм	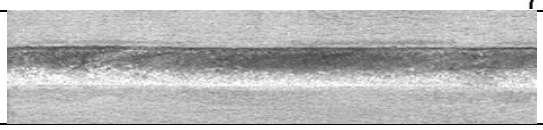

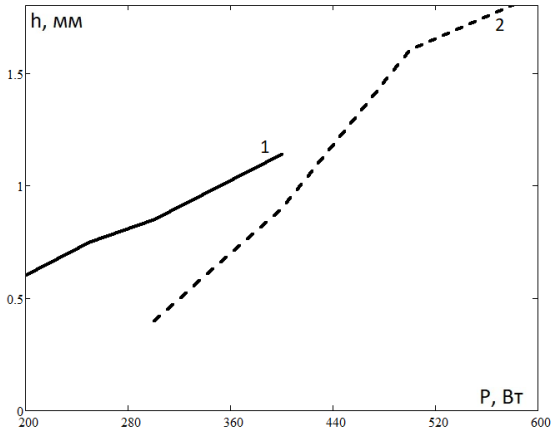

Fig. 6. Dependence of the penetration depth h [mm] of 5083 alloy samples (δ = 2 mm) on the laser radiation power P_L [W] of the fiber laser during welding: 1 – laser-plasma welding (v_w = 4 m/min, I = 50 A, U = 26 V); 2 – laser welding (v_w = 3 m/min).

4.2. Determination of the metallurgical features of the formation of compounds by the laser method.

The main features of weld formation with partial penetration by the laser method are associated with the stability of the existence of the steam-gas channel. It is obvious that the decrease in the value and increase in the frequency of pulsations of this channel contribute to the improvement of penetration formation. The presence of a steam-gas channel contributes to the formation of deep penetration, a distinctive feature of which is the excess of depth over width (Fig.7,a). In this case, the penetration depth was 0.68…0.74 mm, and the width was 0.65…0.70 mm. Along the fusion line, elongated dendritic grains are observed, which makes it possible to speak of a fusion zone 12–16 μm wide (Fig.7b).

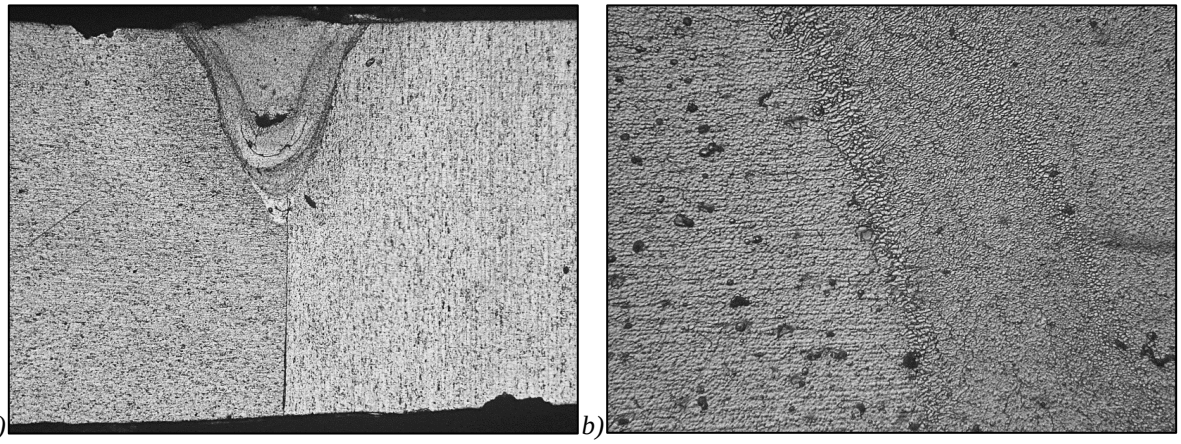

a) *b)*

Fig.7. – General view (a, ×50) of laser penetration and fusion zone (b, ×500) with the base metal.

In the remelted metal, individual pores with a diameter of about 10 μm are observed. Below the middle of the weld, a cavity about 25 × 100 μm in size and microcracks surrounding it with a length of L_{cr} = 25–30 μm were revealed (Fig. 3a). The total volume fraction (V_D) of defects in the weld metal is about 5%. In the center of the weld metal, an equiaxed structure with a grain size of Dg = 10…25 μm (Fig. 7). Microhardness in the center of the weld is HV = 1130…1140 MPa (Fig. 4). Closer to the fusion line in the remelted metal, there is a structure with elongated grains having a size of Dg = (10…15)×(30…35) μm at HV = 980 MPa (Fig. 8, 9). In the lower part of the remelted metal, precipitates of an oxide film were revealed, repeating the shape of the fusion line in the root part. These line-type oxide segregations with the size l_{Al2O3} = 25…35 μm are located in the form of chains up to $L_{\Sigma Al2O3}$ = 50…120 μm (Fig.8a).

The width of the HAZ is h_{HAZ} = 130…150 μm (Fig. 7). The grain size in the HAZ is Dg = (5…20)×(26…50) μm, the grain shape factor ϖ = l/h = 2.5…5. Microhardness compared to the remelted and base metal is increased to HV = 1190…1350 MPa (Fig. 9). In the HAZ near the fusion line, individual microcracks with a length of L_{cr} = 10–20 μm are observed (Fig. 8b).

In the area where two plates of alloy 7075 are joined, the grain size is Dg = (5…15)×(40…70) μm on the side of the left plate and Dg = (5…15)×(30…35) μm on the side of the right one (Fig. 7, a). There is a good connection of the plates without the formation of a gap.

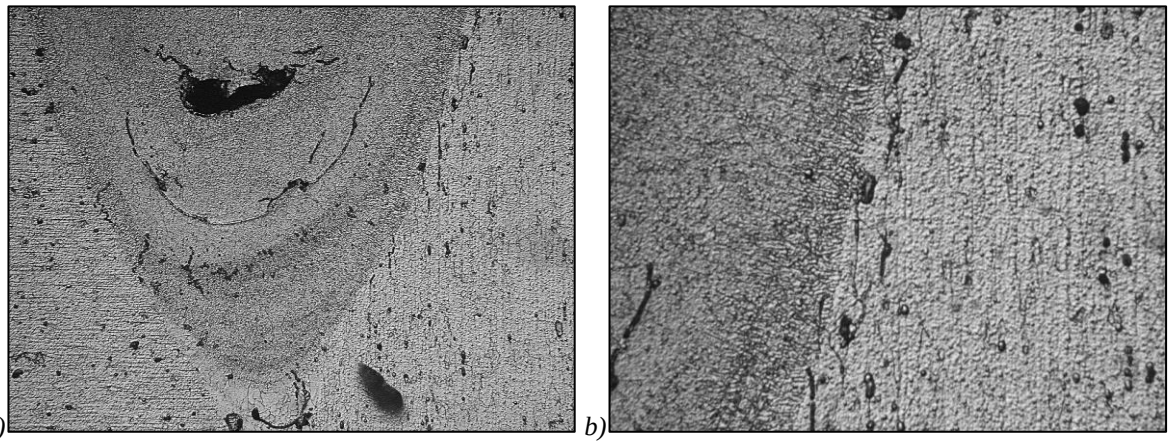

a) *b)*

Fig.8. – Defective areas in laser-remelted metal (a, ×250) and in the base metal near the fusion line (b, ×500).

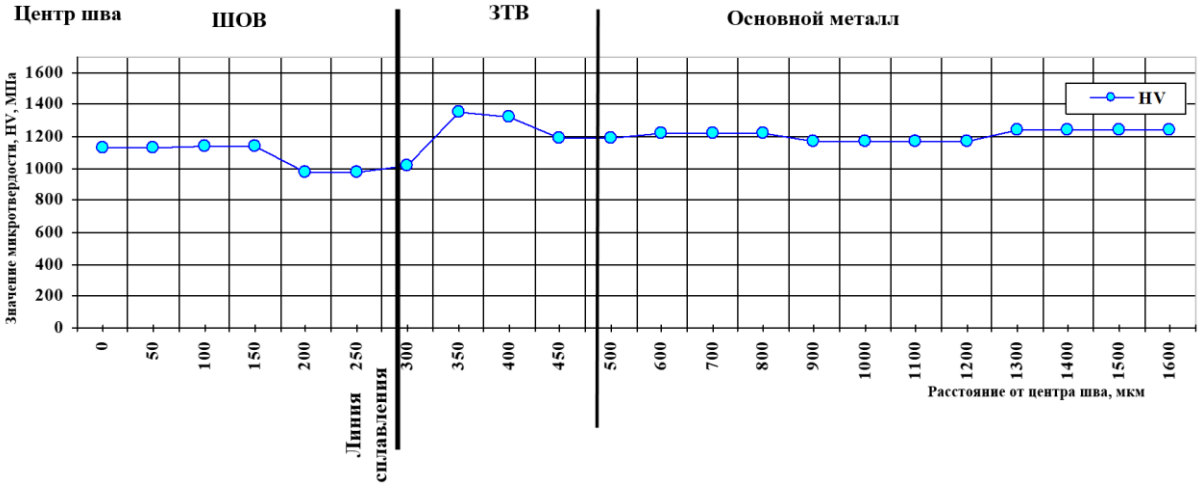

Fig.9.

Distribution of hardness from the axis of penetration towards the base metal in a joint made by a laser method.

Studies of the content of individual elements in the metal of the compound and the base metal by analytical scanning electron microscopy were carried out both integrally over the area of the corresponding zone and in the volume of individual grains. General (integral) studies have shown a tendency to increase the content of Zn in the HAZ. Local analysis of the content of elements in the volume of grains showed an increase in the content of Cu and Zn in the remelted weld metal.

4.3. Determination of metallurgical features of formation of joints by laser-plasma method.

Main features of formation of partial penetration by laser-plasma method are associated with local plasma heating of the formation zone of the steam-gas channel. In this case, the proportion of laser radiation absorbed by the metal increases, the existence of the channel stabilizes, and there is a certain pressure of the electric arc on the melted metal. When using this hybrid welding method, penetration can be formed both closer to laser and plasma. In the experiments, the penetration depth was 0.55...0.56 mm, and the width was 1.0...1.1 mm (Fig. 10, a). The fusion line is quite clearly expressed, but at high magnifications it can be considered as a zone about 15–20 μm wide (Fig. 10b).

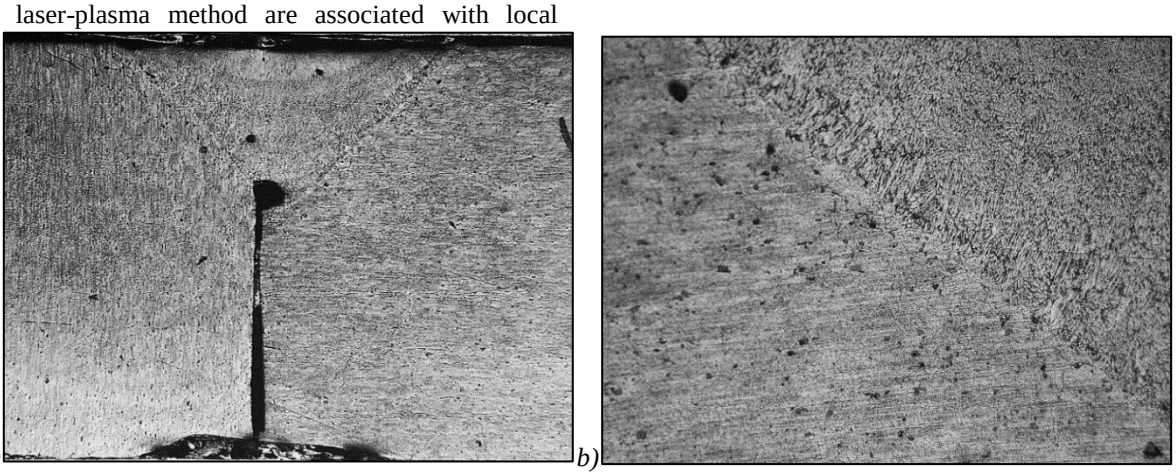

a) *b)*

Fig.10. – General view (a, ×50) of laser-plasma penetration and fusion zone (b, ×250) with the base metal.

In remelted metal, individual pores with a diameter of 15...25 μm are observed (Fig. 11, a). At the weld root, there is a rounded cavity with a diameter of about 100 μm (Fig. 11b). Microcracks around the cavity were not observed. In the central part of the remelted metal, a dispersed structure of an equiaxed shape with a grain size of Dg = 5–15 μm is observed (Fig. 11a). Microhardness in the center of the weld is HV = 896…1180 MPa (Fig. 12). Closer to the fusion line in the remelted metal, an elongated structure is observed with a grain size Dg = (5…10)×(15…60) μm and a hardness HV = 876…916 MPa (Fig. 11b, Fig. 12). In the weld metal, single inclusions of a globular shape 15–25 μm in size were found (Fig. 11b).

The HAZ width is h_{HAZ} = 140…200 μm. The grain size in the HAZ is Dg = (5…10)×(20…50) μm, and the microhardness increases compared to the remelted metal to HV = 876…916 MPa (Fig. 12).

In the joint area of two plates of alloy 7075, the grain size of the metal is: for the left plate Dg = (5…15)×(20…30) μm, and for the right one Dg = (5…6)×(20…30) μm. Between two welded plates, the formation of a gap 10 ... 20 μm wide is observed, which starts directly from the penetration root (Fig. 10, a).

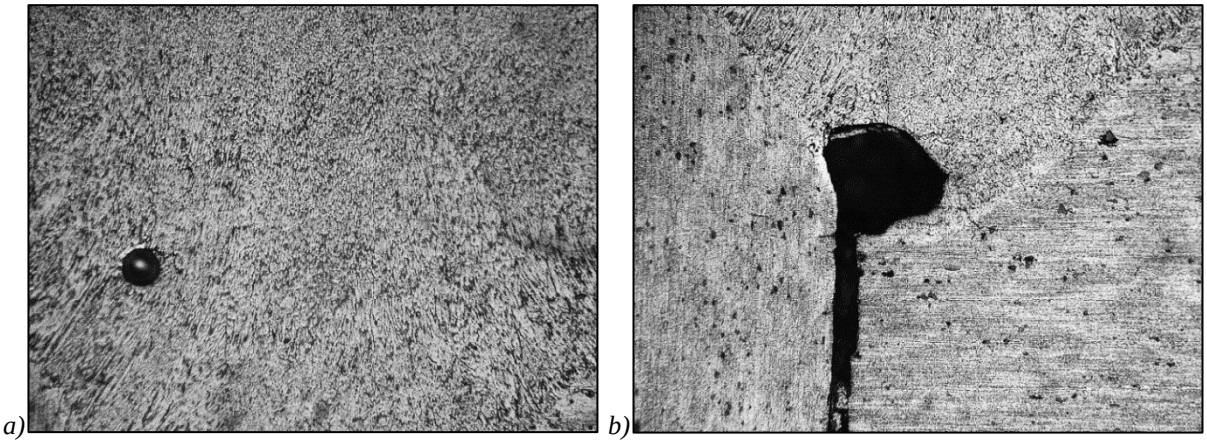

a) *b)*

Fig.11. – Defective areas in the metal remelted by the laser-microplasma method: individual pores (a) and a cavity in the root zone (b), ×250.

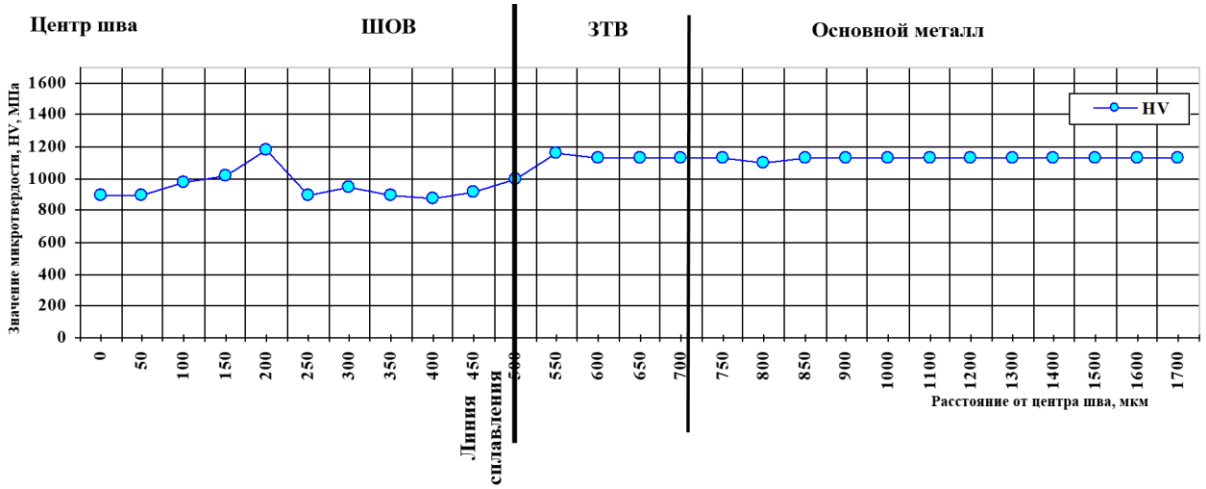

Fig.12. – Distribution of hardness from the axis of penetration towards the base metal in a joint made by the laser-microplasma method.

Studies of the content of individual elements in the metal of the compound and the base metal by analytical scanning electron microscopy were carried out integrally over the area of the corresponding zone, as well as locally in the volume of individual grains and along their boundaries. Both integral and local studies have shown that the content of the analyzed elements in the remelted metal and in the HAZ is approximately at the level of the base metal. In the remelted metal, a slight (about 2%) decrease in the Zn content can be noted, and in the HAZ, its increase by ~7%. Separate inclusions with a high content of Cu (3.83%) and Zn (13.59%) were revealed in the remelted metal. Various inclusions were also found in the HAZ: some with an increased content of Mg (3.57%), Si (4.25%), Cu (3.74%) and Zn (10.65%), others with an increased content of Mg (3 .11%), Mn (2.35%), Cu (4.82%), Zn (13.59%) and Cr (12.57%).

5. Discussion of the results.

It is determined that the influence of the plasma component of the hybrid process led to an increase in the penetration depth by 10...50% without taking into account the difference in welding speeds (Fig. 6). At the same welding speeds, it is possible to predict an increase in the depth of hybrid penetration by 15–65% compared to the laser process.

In studied samples, the base metal has differences in hardness parameters and grain sizes. The spread in

hardness is up to 10%, in grain size - up to 1.5 times or more, in grain shape coefficient $\varnothing$ = 2.5 ... 3.5. In addition, the base metal grains contain inclusions of such elements as Mg, Si, Mn, Cu, Zn, Cr, Fe, with significant deviations from the passport data. In all likelihood, this feature manifested itself in a change in the content of these elements in the remelted weld metal and in the HAZ.

In samples of joints made by the laser method, the depth of penetration varies up to 10% in various sections of the weld. In this case, the width of the HAZ decreases in direct proportion to the decrease in penetration depth from 200...240 μm to 130...150 μm (ie by 30...60%). The total volume fraction of defects (mainly pores 10–30 μm in size) in the remelted metal is about $V_D \sim 5\%$. In the lower third of the remelted metal, there is a cavity approximately 25×100 μm in size, which serves as the center for the initiation of hot cracks with a length of L_{cr} = 25–30 μm. In all likelihood, the formation of this cavity is associated with the ingress of gas from the joint being welded. The gas forms bubbles that do not have time to rise due to the small values of heat input (5 J/mm) and the lifetime of the liquid metal bath (about 0.02…0.04 s). For the same reason, a gap does not have time to form between the joined plates in the unmelted part.

In the root zone of the remelted metal, precipitates of an oxide film were found, repeating the shape of the fusion line. These are line-type precipitates l_{Al2O3} = 25…35 μm in size arranged in the form of chains up to $L_{\Sigma Al2O3}$ = 50…120 μm. Their location is associated with hydrodynamic flows in the liquid metal bath. The grain size in the joint is approximately the same, along the fusion line the shape factor $\varnothing$ = 2…3, in the HAZ $\varnothing$ = 2.5…5. In the remelted metal, closer to the fusion line, the hardness decreases by 10...15%. In the HAZ, the metal hardness increases by about 8...12%. This increase in hardness can contribute to the formation of individual microcracks with a length of L_{cr} = 10–20 μm in the base metal near the fusion line. The absence of a gap between the plates being connected indirectly indicates the presence of internal residual stresses. Relaxation of such stresses can occur in the area of increased hardness of the HAZ with the formation of microcracks (Fig. 8b).

During laser welding, some redistribution of alloying elements of the welded alloy is observed. So, according to the integral indicators, the content of Cu in the remelted metal increases (by ~15%), and in the HAZ metal – Cu (by ~15%) and Zn (8...10%). This can be explained by dissolution with redistribution at the integral level and/or redistribution within the grain boundaries of inclusions present in the base metal.

In samples of joints made by the laser-plasma method, the penetration depth varies within the range of up to 2%. The width of the HAZ is also quite stable – up to 200 μm. The total volume fraction of defects (mainly pores 15–25 μm in size) in the remelted metal is up to $V_D \sim 5\%$. In the root zone of the remelted metal, a cavity is observed, the size of which in various sections varies from round 100×100 μm to oblong 30×100 μm. In all likelihood, the formation of a cavity is associated with the ingress of air from the welded joint. Bubbles are formed that do not have time to rise due to the short time of existence of the molten metal bath (0.03 ... 0.05 s). Traces of the oxide film were not revealed, since the cathodic destruction of the oxide film occurred due to the influence of the plasma component of the process.

The grains in the central part of the remelted metal have an equiaxed shape with a size of Dg = 5…15 μm. Closer to the fusion line in the remelted metal, a structure with more elongated grains is observed, having a shape factor $\varnothing$ = 3…6. In the HAZ, the grain shape factor is $\varnothing$ = 4…5. Compared to the base metal, the microhardness of the remelted zone is reduced by 15...20%, there are separate areas without a decrease in hardness. In the HAZ, the microhardness approximately corresponds to the base metal. This is explained by three times higher heat input (15 J/mm) compared to laser welding (5 J/mm) (Table 1).

In laser-plasma welding, the content of the analyzed elements in the remelted metal and in the HAZ is approximately at the level of the base metal. The exceptions are the decrease in the Zn content (about 2%) in the remelted metal and its increase (by ~7%) in the HAZ. Separate inclusions with a high content of Mg, Si, Mn, Cu, Zn and Cr were found in the remelted metal and in the HAZ. Their presence, in all likelihood, is explained by the presence of similar inclusions in the base metal.

6. Conclusions.

1. The use of concomitant plasma heating in laser welding makes it possible to increase the penetration depth by 15–65% compared to conventional laser welding, including by improving of radiation absorption. To improve the absorption of radiation during laser-plasma welding, the distance between the center of the anode region of the compressed arc of the nonconsumable electrode and the laser radiation axis should not exceed 1.0 mm. To establish a full-fledged hybrid laser-plasma process, this distance should not exceed 0.5 mm.

2. Application of laser radiation in welding of 7075 alloy makes it possible to obtain joints with sufficiently narrow seams with minimal input energy and the lifetime of the melt pool. The grain size of the joint is regular, equiaxed in the remelted metal and elongated along the fusion line ($\varnothing$ = 2…3) and in the HAZ ($\varnothing$ = 2.5…5). The microhardness of the remelted metal decreases by 10...15%, and in the HAZ it increases by 8...12% relative to the base metal. The elongated shape of the grains and the increase in hardness can explain the appearance of microcracks 10–20 μm long in the HAZ. Another disadvantage of laser welding is the release of an oxide film in the root of the remelted metal.

3. The use of concomitant local plasma heating during laser welding of the 7075 alloy ensures the production of welds ~1.5 times wider than laser welds. The grain size of the joint is reduced. The grain structure of the remelted metal has an equiaxed structure, the grain size is reduced by 1.5-2 times compared to laser welding. Structures with elongated grains are formed along the fusion line and in the HAZ ($\varnothing$ = 3…6 and $\varnothing$ = 4…5, respectively). The microhardness of the remelted metal is reduced by 15...20%, and in the HAZ approximately

corresponds to the base metal. The reduction in graininess and increase in the uniformity of joint hardness, combined with the elimination of the formation of microcracks and oxide inclusions, makes the hybrid welding method preferable.

References:

1. Nele, L., Mattera, G., Vozza, M. (2022). Deep Neural Networks for Defects Detection in Gas Metal Arc Welding. Appl. Sci., 12, 3615.

2. Moglia, F., Raspa, A. (2020). New Trends in Laser Beam Welding: How automotive applications are driving the future of laser technologies // Photonics Views, 17(5), 26-29.

3. Krivtsun, I.V., Khaskin, V.Yu., Korzhik, V.N., Luo, Z. (2015). Industrial application of hybrid laser-arc welding (Review) // The Paton Welding Journal, 7, 41-46.

4. Bushma, O. (2015). State-of-the-art of hybrid laser-plasma welding (Review) // The Paton Welding Journal, 8, 18-25.

5. Bunaziv, I., Akselsen, O. M., Ren, X., Nyhus, B., Eriksson, M. (2021). Laser Beam and Laser-Arc Hybrid Welding of Aluminium Alloys // Metals, Vol. 11(8), pp. 1150.

6. Korzhyk, V.M., Khaskin, V.Yu., Peleshenko, S.I., Grynyuk, A.A., Chunlin, D., Illyashenko, E.V., Yao, Y. (2022). Selection of parameters of laser welding of thin-walled items from light alloys with nonthrough thickness penetration // The Paton Welding Journal, 5, 16-25.

7. Sokolov, M., Salminen, A. Improving Laser Beam Welding Efficiency // Physics Procedia, 6(09), pp. 559-571. (2014).